Available online at www.sciencedirect.com

ScienceDirect

Ceramics International 41 (2015) 2840–2846

CERAMICS INTERNATIONAL

www.elsevier.com/locate/ceramint

Performance of TBCs system due to the different thicknesses of top ceramic layer

Xufei Fang, Guobing Zhang, Xue Feng*

AML, Department of Engineering Mechanics, Tsinghua University, Beijing, 100084, China

Received 22 September 2014; received in revised form 15 October 2014; accepted 15 October 2014
Available online 24 October 2014

Abstract

Yttria-stabilized zirconia (YSZ) thermal barrier coatings (TBCs) with thicknesses of 200μm and 400μm were sprayed using supersonic plasma spraying (SPS) on FeNi-based substrate and Ni-based substrate, respectively. Bonding strengths of FeNi-based substrate and Ni-based substrate with different thicknesses of coatings were investigated. Bonding strength tests revealed different fracture mechanisms for the specimens with thin topcoat and thick topcoat. Scanning electron microscope (SEM) and metallographic microscope observation of the crossing sections revealed that the porosity of the thin coating was smaller than that of the thick coating, and the distribution of the porosity further determines the location of the fracture zones. Thermally grown oxide (TGO) with different thicknesses grows on the interface of the bond coat (BC) and top ceramic layer due to oxidation. Analysis validates that thickness of the topcoat plays an important role in the diffusion of oxygen and oxidation rate of the TGO while the porosity has little effect on the oxidation rate.

Keywords: Thermal barrier coating; Ceramic layer thickness; Porosity; Oxidation

1. Introduction

Thermal barrier coatings (TBCs) are of great importance in engineering applications, such as engine turbines, to improve the performance of metallic substrates at high temperature [1–3]. Yttria-stabilized zirconia (YSZ) materials have been widely used as the ceramic topcoat of TBC systems. The basic structure for TBCs consists of three layers, namely, the bond coat (BC), thermally grown oxide (TGO) and top ceramic layer [3,4]. The low thermal conductivity of the top ceramic layer enables it to protect the substrate from the outside high temperature gas and to improve the durability of the turbine blades and extend the service life of the turbine engines [3,5,6]. There have been intensive studies on the fabrication, stress measuring and structural design of coatings to improve the properties of TBCs due to its importance [7–16]. However, the areas of mechanical properties, failure mechanism and lifetime prediction are still being widely studied. There are still continuous efforts dealing with nano-sized particle research[17], multi-layer composition [18,19] and gradient design technique, etc. Meanwhile, new material systems, for instance, rare earth $La_2Zr_2O_7$ based TBCs or $La_2(Zr_{1-x}Ce_x)_2O_7$ based TBCs are still being developed[20].

As mentioned above, the top ceramics layer plays a very important role in protecting the substrate. The microstructure and thickness of the top ceramic layer have great influences on its properties [21], such as the thermal conductivity and the oxygen diffusion coefficient, which affect the growth rate of TGO forms at the BC surface by reaction with the combustion gas. For TBC fabrication, there are currently two main methods that are used, namely, atmospheric plasma spraying (APS) [22] and electron beam physical vapor deposition (EBPVD) [23]. The differences in the microstructures of the coatings produced using the above two methods cause different porosity percentages, thermal conductivity coefficients and strain compliance effect when the materials are subjected to high temperature [6].

However, for the top ceramic layer, there is a lack of research focusing on the effect of its thickness on the microstructure and diffusion properties, especially on the oxidation evolution process of the TGO. In this work, we developed TBCs with different

*Corresponding author. Tel.: +86 (10)62781465; fax: +86-(10)62781465.
E-mail address: fengxue@tsinghua.edu.cn (X. Feng).

http://dx.doi.org/10.1016/j.ceramint.2014.10.105
0272-8842/

thicknesses (i.e. 200 μm and 400 μm, respectively) by using supersonic plasma spraying (SPS) [24–26] on Ni-based substrate and FeNi-based substrate, respectively. The effects due to the different thicknesses on the properties of the TBC system were comprehensively studied. The micro porosities in the top coatings with two different thicknesses were measured and the influence on the oxygen diffusion and the growth rate of TGO were also investigated. An oxidation model was developed to study the oxide growth rate with different thicknesses and porosity percentage to validate the experimental results. Results in this work are expected to provide guidance for the evaluation and determination of the thickness of the top ceramic layer and also provide information about the failure mechanism, especially for the oxidation mechanism due to the thickness and porosity of the top layer.

2. Experimental procedure

2.1. Preparation of specimens

Two categories of substrates (i.e. Fe-Ni-based substrate, Ni-based substrate) were investigated. The substrates were cut into plates with a thickness of 6 mm and a diameter of 30 mm and then were polished to remove the remnant oil and oxide films. Then the surfaces of the specimens were coarsened to increase the contact area as well the adhesion properties between coatings and substrates by using sand blasting with a pressure of 0.4 MPa. Then the substrates were coated with NiCrCoAlY (mean particle size 45μm) as the adhesive layer with a thickness of approximately 50 μm. Finally, ceramic layers with thicknesses of about 200 μm (thin layer) and 400 μm (thick layer) were coated by using SPS. The velocities of the particles can be significantly increased and are expected to form a more compact coating [24–26].

The ceramics layers were deposited by using nano size YSZ (7%Wt Y_2O_3) powders (mean particle size 50–100 nm), which were reprocessed to form micro granules with mean sizes in the range of 30–50 μm for a better spraying quality of the coatings [27].

2.2. Characterization and mechanical tests

The surface of the prepared specimens was analyzed by scanning electron microscope (SEM). The bonding strength of the top ceramic coatings on the prepared substrates was tested by using bonding strength test based on ASTM C633-79 standard. The average diameter of the specimens is 25.0 mm. Both surfaces of the specimens were firmly attached to the fixtures (stainless steel rods) at both ends by using engineering glue. The test results and metallographic observation for top ceramic coat with two different thicknesses on FeNi-based substrate and Ni-based substrate were compared. The results are shown below in the analysis part.

2.3. Isothermal oxidation

TBC systems were exposed to high temperature environment and oxidation is among one of the most serious problems. The thickening of the highly stressed TGO has a crucial influence on the stability and durability of the TBC system [3,4,28–30]. Thus it is of great necessity to study the oxidation evolution of the TGO in the TBC system with different top coat thicknesses. In what follows we compared the oxide growth rate for coatings with different thicknesses on the FeNi-based substrates. The specimens were placed in a furnace at temperature of 1000 °C. The thicknesses of the TGO were measured and compared by using metallographic observation on the cross-section of the specimen after the experiment. Furthermore, a theoretical model for oxidation was carried out taking into account the influence of the thickness and porosity of the top ceramic layer to compare the predicted data with the experimental results.

3. Results and analysis

3.1. SEM observation of the top ceramics layer

As shown in Fig. 1, the top coat layer has a rough surface. In Fig. 1 (b) the surface morphology exhibits clearly a melted feature. This is due to the high temperature in the supersonic

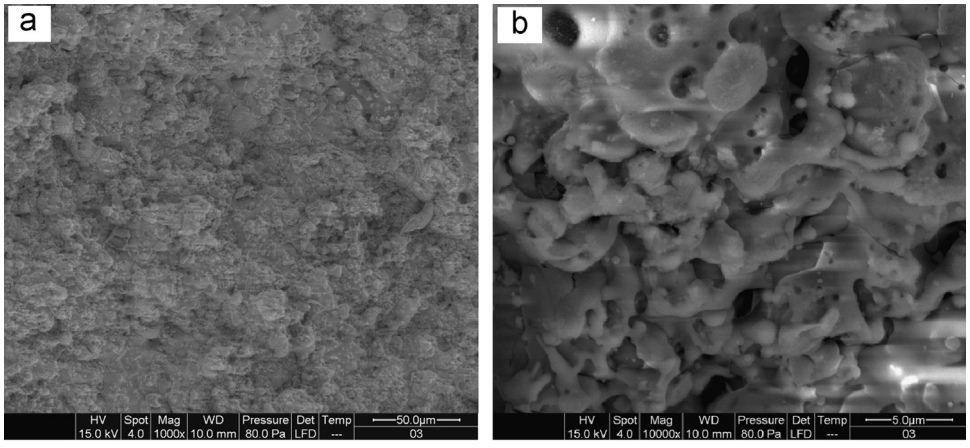

Fig. 1. SEM morphologies of the surface.

Table 1
Results of bonding strenght tests.

	Maximum tensile load/KN	Bonding strength/MPa	Dominant fracture mechanisms
FeNi substrate +thin coating(200μm)	20.465	10.853	Interface spallation between adhesive layer and top ceramic layer
FeNi substrate +thick coating(400μm)	20.423	10.830	Internal fracture within the top ceramics layer
Ni substrate +thick coating(400μm)	10.021	8.820	Internal fracture within the top ceramics layer

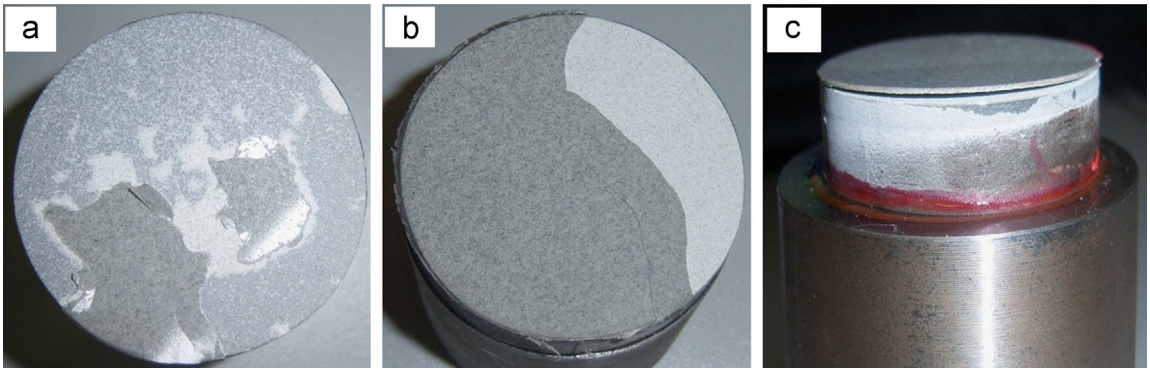

Fig. 2. Surface of specimens after bonding test: (a) FeNi substrate and thin coating; (b) FeNi substrate and thick coating; (c) Ni substrate and thick coating.

spraying process on the surface, which could be as high as 3100 °C [24]. As indicated in the experiment part, the particles of the ceramic layer were made of micro-size particle, which are granules originally from nano-size particles [27].

3.2. Bonding strength test: Macroscopic observation of the fracture surface

Results of the bonding strength tests in Table 1 show that the bonding strengths are almost same for FeNi-based substrate sprayed with thin coating and thick coating. However, the locations of the fracture zones are different for two types of coatings. For the specimens with thin coating, the fracture occurs mainly on the interface between the adhesive layer and the top ceramic layer, while for the specimens with thick coating, the fracture occurs mainly within the top ceramic layer itself, as illustrated in Fig. 2. The results for FeNi-based and Ni-based specimens with thick coatings show consistently this phenomenon. This difference of the fracture mechanism is analyzed later.

3.3. Metallographic observation of the cross-sections

The cross-sectional metallographic images of FeNi-based specimens and Ni-based specimens are presented in Figs. 3 and 4, respectively. The percentage of defects and porosity in Figs. 3 and 4 are averagely much higher for thick coatings (for both FeNi-based specimens and Ni-based specimens) than those of thin coatings. For the thick coatings in Fig. 3(a) and Fig. 4(a), the porosity density increases as it approaches the surface of the topcoat. Near the BC and the substrate, as indicated in Fig. 3(a) and Fig. 4(a), where it is above the blue line, the structure and porosity density of the thick top ceramic layer is similar to those of the thin top layer, which is shown consistent for both types of specimens. Above the blue line approaching the BC and substrate, the porosity in the coating is rather low. And it is also observed that the distance from the blue line to the BC for thick coatings is almost the same as the thickness of the thin top coat, which is approximately 200μm. Whilst below the blue line, the porosity in the thick coating increases sharply and more defects are observed. The consequences of such a structure in the thick coatings, as shown in Fig. 3(a) and Fig. 4(a), is that with thermal cycling the defects in the thick top coatings could coalescence with each other and form defects with a width at the scale of tens of micrometer or even larger[31], which can be catastrophic for the rupture of the BC, as verified by the fracture observation and bonding strength in the above bonding strength tests. The following analysis in Section 3.4 reveals that this structure and porosity distribution cause the fracture zone to distribute differently for thick and thin coatings.

3.4. SEM morphologies of the fracture surface: within the coating ceramic layer

As shown in Fig. 5, with the red ellipses and arrows indicating the facture surfaces and cavities respectively within the fracture zone, the crack surfaces are perpendicular to the loading direction. The loading direction was perpendicular to the surface of the topcoat, namely, the loading direction is parallel to the particle spraying direction. Meanwhile, the crack surfaces observed are smooth, which indicates that this type of crack surfaces originate from these porosities existed during the praying process in the thick coatings, where small cracks propagate and coalesce to form larger cracks [29]. Although the porosity can help to improve the lateral strain compliance of the coating at high temperature and maintain the stability of

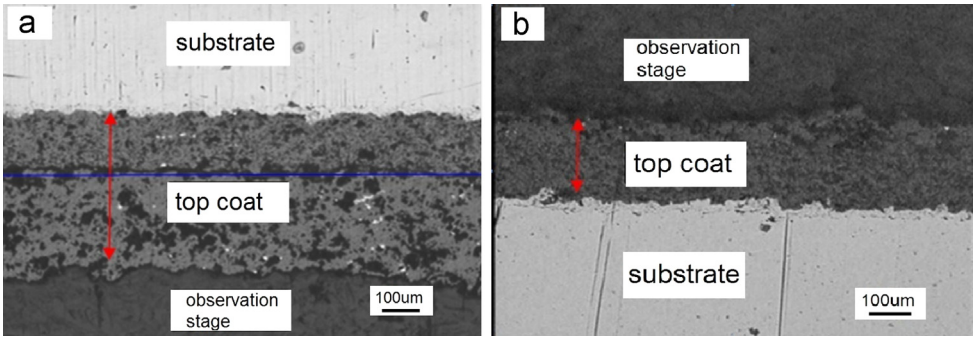

Fig. 3. Crossssectional metallographic images of FeNi-based specimens: (a) thick topcoat; (b) thin topcoat.

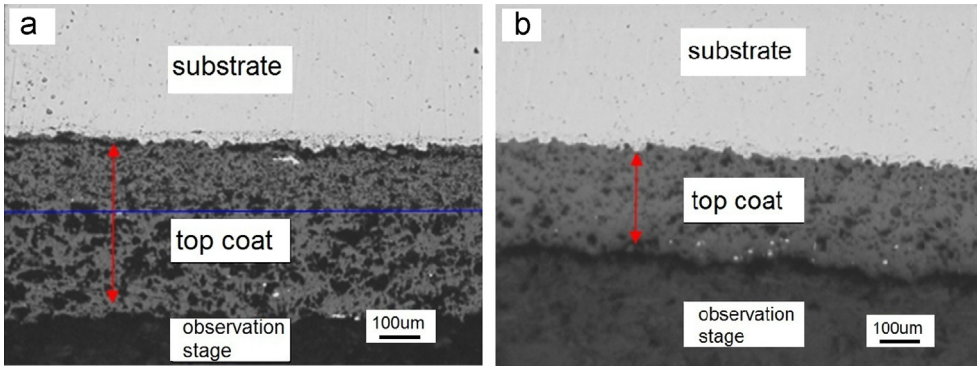

Fig. 4. Cross-sectional metallographic images of Ni-based specimens: (a) thick topcoat; (b) thin topcoat.

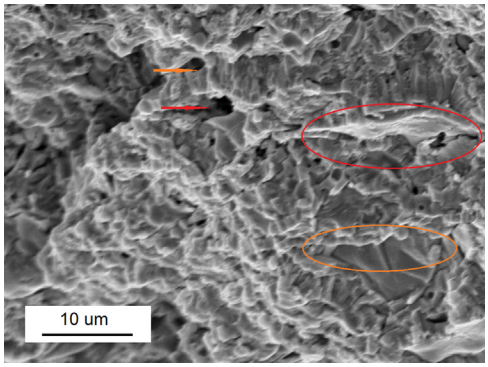

Fig. 5. SEM morphologies of the fracture surface: within the top ceramic layer.

the coating [3], the evidence in Figs. 3 and 4 shows that defects and porosities are the major resources for cracks, which further lead to the fracture of the coating system under certain conditions.

3.5. Oxidation study

As shown in Fig. 6, the cross-sectional images of FeNi-based specimens after oxidation show a typical three layer of the TBC system at high temperature, namely, the top ceramic layer, the TGO and BC (the adhesive layer). The average TGO thickness for thin topcoat and thick topcoat is about 18 μm and 12 μm, respectively. Though a bit thicker, still it is near the typical range of TGO thickness [29]. As can be noticed, due to the surface roughness of the BC, the thickness of the TGO is not equally distributed along the interface of the topcoat and BC. Moreover, based on the above observations of the different distribution of the porosities within the thick and thin top ceramic layers, it is yet unclear how the existence of this porosity as well as the thickness of the ceramic layer would affect the diffusion coefficient of the oxygen and the growth rate of the oxide.

In order to validate this explanation, we propose a model in what follows to demonstrate the influence of the porosity and thickness on the oxide growth rate.

Assume that the oxidation is mainly controlled by the diffusion of oxygen and the interfaces are smooth under an ideal condition. The TGO (indicated as “b” in Fig. 7) grows at the interface of the top ceramic layer (indicated as “a” in Fig. 7) and BC (indicated as “a” in Fig. 7, where the spots and lines indicate the porosity in the top ceramic layer) involves counter-diffusion of oxygen and aluminum along the α-Al_2O_3 grain boundaries. The porosity in the top ceramic layer (which is very common and unavoidable due to the fabrication techniques in plasma spraying) would have an influence on the diffusion coefficient for the oxygen transmitted to the TGO upper surface (interface of ceramic layer and TGO, denoted as interface I), and further transmitted to the TGO bottom surface (interface of TGO and BC, denoted as interface II). The interface of TGO and BC is supposed to be the oxidation frontier where oxidation occurs and oxide scale grows [28–30]. Here we assume that the oxidation in top ceramic layer and on the interface of the TGO and top ceramic is negligible.

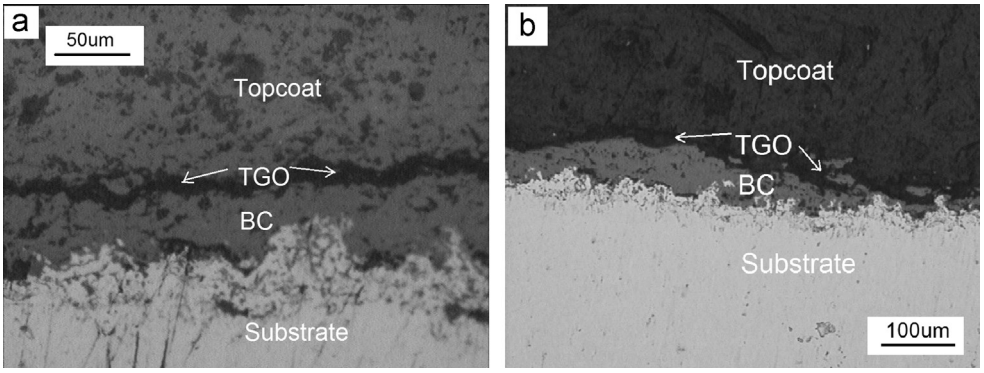

Fig. 6. Oxidation of FeNi-based specimen at 1000 °C: (a) thin topcoat; (b) thick topcoat.

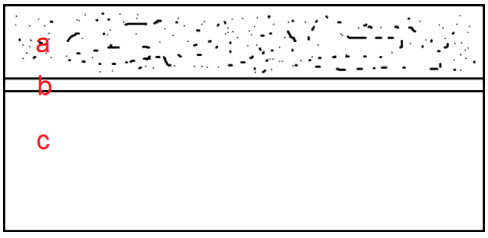

Fig. 7. Schematic of TGO growth in TBC system on substrate.

Assume that the whole system is in thermodynamic equilibrium and apply Fick's first law to the interface I and interface II respectively and it yields to [32]:

$$j_o^I = D_h \frac{C_o^{air} - C_o^I}{h \cdot f(p)} \tag{1}$$

$$j_o^{II} = D_{ox} \frac{C_o^I - C_o^{II}}{\delta} \tag{2}$$

where j_o^I and j_o^{II} are the fluxes of oxygen on interface I and interface II, respectively. D_h is the diffusion coefficient of the top ceramic layer, D_{ox} is the diffusion coefficient of the oxide layer (TGO), C_o^{air} is the oxygen concentration in air on the outer surface of the top ceramic layer, C_o^I and C_o^{II} are the oxygen concentrations on the interface I and the interface II, respectively, h is the thickness of the top ceramic layer, δ is the thickness of the TGO (here we take δ as an average thickness for simplicity) and $f(p)$ is the function for characterizing porosity (p). Here the term $h \cdot f(p)$ in Eq. (1) can be viewed as the equivalent thickness of the top ceramic layer due to the existence of porosity. For simplicity, we give one candidate for the expression of $f(p)$:

$$f(p) = 1 - p \tag{3}$$

where p is the porosity percentage ($0 < p < 1$). It can be seen that the higher the porosity, the smaller the equivalent thickness of the top ceramic layer is.

Meanwhile, concerning the TGO growth rate to the oxygen flux on interface II, we have [32]:

$$j_o^{II} = D_{ox} \frac{C_o^I - C_o^{II}}{\delta} = \frac{d\delta}{dt} \frac{1}{V_{ox}} \tag{4}$$

where V_{ox} is the molar volume of the oxide layer (TGO) and t is time.

Considering the thermodynamic equilibrium state of the system, the flux on interface I and interface II should be equal so that there would not be extra oxygen accumulating on the interface I. This also means that the consumption of oxygen on interface II equals to the supply of oxygen on interface I. Thus we have:

$$j_o^I = j_o^{II} \tag{5}$$

By using Eqs. (1), (2) and (5), we can get the explicit expression of C_o^I, which is the oxygen concentration on interface I:

$$C_o^I = \frac{\delta D_h C_o^{air} + D_{ox} h \cdot f(p) C_o^{II}}{\delta D_h + D_{ox} h \cdot f(p)} \tag{6}$$

Substitute Eq. (6) into Eq. (4), it yields to:

$$\frac{d\delta}{dt} = \frac{V_{ox} D_{ox} D_h (C_o^{air} - C_o^{II})}{\delta D_h + D_{ox} h \cdot f(p)} \tag{7}$$

By using the initial condition $\delta = 0$ when $t = 0$, and we get:

$$\frac{\delta^2}{2} D_h + D_{ox} h \cdot f(p) \cdot \delta = V_{ox} D_{ox} D_h (C_o^{air} - C_o^{II}) \cdot t \tag{8}$$

Solve Eq. (8) we can get the expression for TGO thickness:

$$\delta = \frac{-D_{ox} h \cdot f(p) + \sqrt{[D_{ox} h \cdot f(p)]^2 + 2 V_{ox} D_{ox} D_h^2 (C_o^{air} - C_o^{II}) \cdot t}}{D_h} \tag{9}$$

Since the porosity of the top ceramic layer can influence the diffusion coefficient, namely, D_h, of the top ceramic layer, we assume that the higher the porosity, the smaller the diffusion coefficient it has. For simplicity, we adopt the same function of Eq. (3) for the expression of D_h for instance:

$$D_h = D_{h0} \cdot f(p) = D_{h0} \cdot (1 - p) \tag{10}$$

where D_{h0} stands for ideal diffusion coefficient for the top ceramic layer without porosity.

Substitute Eq. (10) into Eq. (9), we have:

$$\delta = \frac{-D_{ox} h + \sqrt{(D_{ox} h)^2 + 2 V_{ox} D_{ox} D_{h0}^2 (C_o^{air} - C_o^{II}) \cdot t}}{D_{h0}} \tag{11}$$

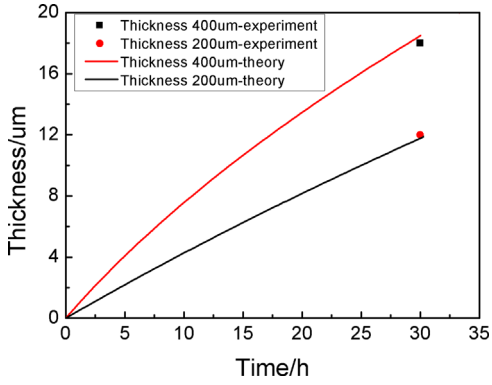

Fig. 8. Thickness evolution of TGO with different coating thicknesses.

As indicated by Eq. (11), when the function of porosity was chosen to be as Eq. (3), the porosity would not influence the oxidation growth rate of the TGO. Based on the expression of oxide thickness in Eq. (11), we calculate the TGO thicknesses for different topcoat and the results are shown in Fig. 8. Here h in Eq. (11) is set to be 200μm and 400μm, respectively. For comparison, the experimental data is also shown in Fig. 8. The experimental results agree well with the theoretically predicted results.

4. Conclusions

Yttria-stabilized zirconia (YSZ) thermal barrier coatings (TBCs) with thicknesses of 200μm and 400μm were sprayed using supersonic plasma spraying (SPS) on a FeNi-based substrate and Ni-based substrate, respectively. The thickness of the top YSZ coatings has a great influence on the mechanical properties of the TBCs systems as well as the oxidation rate of the thermally grown oxide (TGO) at the interface of the bond coat and topcoat. Results of bonding strength tests revealed different fracture mechanisms for TBCs system with thin topcoat and thick topcoat. The fracture zones for thick coatings on FeNi-based substrate and Ni-based substrate occur consistently within the top ceramic layer mainly due to the defects and the porosities. Bonding strength of the FeNi-based substrate with thin coating and thick coating are almost the same, but higher than that of the Ni-based substrate with thick coating. The porosity in the thick topcoat is on average larger than that in thin topcoat and the distribution of the porosity in the thick topcoat near the substrates show a similar characteristic to that of the thin topcoat. However, the porosity in the thick topcoat becomes much larger when it approaches the surface of the topcoat. Thickness of the coating influences the oxygen diffusion, which further affects the oxidation rate of the TGO. In contrast, the porosity has little effect on the oxidation rate for the equilibrium state in the present model.

Acknowledgment

We gratefully acknowledge the support from the National Basic Research Program of China (Grant No. 2015CB351904), National Natural Science Foundation of China (Grant Nos. 11222220, 11320101001, 11090331, 11227801) and Tsinghua University Initiative Scientific Research Program.

References

[1] A.G. Evans, D.R. Mumm, J.W. Hutchinson, G.H. Meier, F.S. Pettit, Mechanisms controlling the durability of thermal barrier coatings, Prog. Mater. Sci. 46 (2001) 505–553.
[2] J. Maikell, J. Piggush, A. Kohli, D. Bogard, Experimental simulation of a film cooled turbine blade leading edge including thermal barrier coating effects, J. Turbomach 133 (2010) 011014.
[3] D.R. Clarke, M. Oechsner, N.P. Padture, Thermal-barrier coatings for more efficient gas-turbine engines, MRS. Bull 37 (2012) 891–898.
[4] K.W. Schlichting, N.P. Padture, E.H. Jordan, M. Gell, Failure modes in plasma-sprayed thermal barrier coatings, Mater. Sci. Eng., A. 342 (2003) 120–130.
[5] A.M. Limarga, R. Vaßen, D.R. Clarke, Stress distributions in plasma-sprayed thermal barrier coatings under thermal cycling in a temperature gradient, J. Appl. Mech. 78 (2010) 011003.
[6] S. Sampath, U. Schulz, M.O. Jarligo, S. Kuroda, Processing science of advanced thermal-barrier systems, MRS. Bull 37 (2012) 903–910.
[7] K. Duan, R.W. Steinbrech, Influence of sample deformation and porosity on mechanical properties by instrumented microindentation technique, J. Eur. Ceram. Soc. 18 (1998) 87–93.
[8] X. Feng, Y. Huang, A.J. Rosakis, Multi-layer thin films/substrate system subjected to non-uniform misfit strains, Int. J. Solids Struct. 45 (2008) 3688.
[9] Y. Zeng, S.W. Lee, L. Gao, C.X. Ding, Atmospheric plasma sprayed coatings of nanostructured zirconia, J. Eur. Ceram. Soc. 22 (2002) 347–351.
[10] X. Feng, Y. Huang, A.J. Rosakis, On the stoney formula for a thin film/substrate system with nonuniform substrate thickness, J. Appl. Mech. 74 (2007) 1276.
[11] W.X. Zhang, X.L. Fan, T.J. Wang, The surface cracking behavior in air plasma sprayed thermal barrier coating system incorporating interface roughness effect, Appl. Surf. Sci. 258 (2011) 811–817.
[12] X.L. Fan, W.X. Zhang, T.J. Wang, Q. Sun, The effect of thermally grown oxide on multiple surface cracking in air plasma sprayed thermal barrier coating system, Surf. Coat. Technol 208 (2012) 7–13.
[13] M.P. Schmitt, A.K. Rai, R. Bhattachary, D. Zhu, D.E. Wolfe, Multilayer thermal barrier coating (TBC) architectures utilizing rare earth doped YSZ and rare earth pyrochlores, Surf. Coat. Technol 251 (2014) 56–63.
[14] X. Feng, Y. Huang, A.J. Rosakis, Stresses in a multilayer thin film/substrate system subjected to nonuniform temperature, J. Appl. Mech. 75 (2008) 021022.
[15] X.L. Dong, X. Feng, K.C Hwang, Oxidation stress evolution and relaxation of oxide film/metal substrate system, J. Appl. Phys. 112 (2012) 023502.
[16] Y. Zhao, D. Li, X. Zhong, H. Zhao, L. Wang, F. Shao, C. Liu, S. Tao, Thermal shock behaviors of YSZ thick thermal barrier coatings fabricated by suspension and atmospheric plasma spraying, Surf. Coat. Technol 249 (2014) 48–55.
[17] N.P. Padture, K.W. Schlichting, T. Bhatia, et al., Towards durable thermal barrier coatings with novelmicrostructures deposited by solution-precursor plasma spray, Acta Mater. 49 (2001) 2251–2257.
[18] H. Xu, H. Guo, F. Liu, et al., Development of gradient thermal barrier coatings and their hot-fatigue behavior, Surf. Coat. Technol 130 (2000) 133–139.
[19] X.L. Fan, R. Xu, T.J. Wang., Interfacial delamination of double-ceramic-layer thermal barrier coating system, Ceram. Int. 40 (2014) 13793–13802.
[20] D. Stöver, G. Pracht, H. Lehmann, M. Dietrich, J.E. Doring, R. Vassen., New material concepts for the next generation of plasma-sprayed thermal barrier coatings, J. Therm. Spray. Technol. 13 (2004) 76–83.
[21] X.N. Li, L.H. Liang, J.J. Xie, L Chen, Y.G Wei., Thickness–dependent fracture characteristics of ceramic coatings bonded on the alloy substrates, Surf. Coat. Technol. (2014)http://dx.doi.org/ 10.1016/j.surfcoat.2014.07.031 (in press).

[22] H. Herman, S. Sampath, R. McCune, Thermal spray: current status and future trends, MRS Bull 25 (2000) 17–25.
[23] U Schulz, C Leyens, K. Fritscher, M. Peters, B. Saruhan-Brings, O. Lavigne, J.M. Dorvaux, M Poulain, R. Mevrel, M.L. Caliez, Some recent trends in research and technology of advanced thermal barrier coatings, Aerosp. Sci. Technol. 7 (2003) 73–80.
[24] Y. Bai, Z.H. Han, H.Q. Li, C. Xu, Y.L. Xu, Z. Wang, C.H. Ding, J.F. Yang, High performance nanostructured ZrO_2 based thermal barrier coatings deposited by high efficiency supersonic plasma spraying, Appl. Surf. Sci. 257 (2011) 7210–7216.
[25] H. Wu, H.J Li, C. Ma, Q.G. Fu, Y.J. Wang, J.F. Wei, J. Tao, $MoSi_2$-based oxidation protective coatings for SiC-coated carbon/carbon composites prepared by supersonic plasma spraying, J. Eur. Ceram. Soc. 30 (2010) 3267–3270.
[26] X.C. Zhang, B.S. Xu, Y.X. Wu, F.Z. Xuan, S.T. Tu, Porosity, mechanical properties, residual stresses of supersonic plasma-sprayed Ni-based alloy coatings prepared at different powder feed rates, Appl. Surf. Sci. 254 (2008) 3879–3889.
[27] L.L. Shaw, D. Goberman, R. Ren, M. Gell, S. Jiang, Y. Wang, T.D. Xiao, P.R. Strutt, The dependency of microstructure and properties of nanostructured coatings on plasma spray conditions, Surf. Coat. Technol 130 (2000) 1–8.
[28] A. Rabiei, A.G. Evans, Failure mechanisms associated with the thermally grown oxide in plasma-sprayed thermal barrier coatings, Acta Mater. 48 (2000) 3963–3976.
[29] P.K. Wright, A.G. Evans, Mechanisms governing the performance of thermal barrier coatings, Curr. Opin. Solid State Mater. Sci 4 (1999) 255–265.
[30] R.J. Christensen, V.K. Tolpygo, D.R. Clarke, The influence of the reactive element yttrium on the stress in alumina scales formed by oxidation, Acta Mater. 45 (1997) 1761–1766.
[31] X.L. Fan, W. Jiang, J.G. Li, T. Suo, T.J. Wang, R. Xu., Numerical study on the interfacial delamination of thermal barrier coatings with multiple separations, Surf. Coat. Technol 244 (2014) 117–122.
[32] Neil Birks, Gerald H. Meier, Fred S. Pettit, Introduction to the High-Temperature Oxidation of Metals, 2nd edition, Cambridge University Press, 2006.